Integrated Use of Biochemical, Native Mass Spectrometry, Computational, and Genome-Editing Methods to Elucidate the Mechanism of a *Salmonella* deglycase

Anindita Sengupta[1,†], Jikang Wu[1,‡,§], Justin T. Seffernick[1,‡], Anice Sabag-Daigle[2,‡], Nicholas Thomsen[1], Tien-Hao Chen[1,¶], Angela Di Capua[1], Charles E. Bell[1,3], Brian M.M. Ahmer[2], Steffen Lindert[1], Vicki H. Wysocki[1] and Venkat Gopalan[1]

1 - Department of Chemistry and Biochemistry, *The Ohio State University, Columbus, OH 43210, USA*
2 - Department of Microbial Infection and Immunity, *The Ohio State University, Columbus, OH 43210, USA*
3 - Department of Biological Chemistry and Pharmacology, *The Ohio State University, Columbus, OH 43210, USA*

Correspondence to Venkat Gopalan: *gopalan.5@osu.edu*
https://doi.org/10.1016/j.jmb.2019.08.017
Edited by Patrick Griffin

Abstract

Salmonella is a foodborne pathogen that causes annually millions of cases of salmonellosis globally, yet *Salmonella*-specific antibacterials are not available. During inflammation, *Salmonella* utilizes the Amadori compound fructose−asparagine (F-Asn) as a nutrient through the successive action of three enzymes, including the terminal FraB deglycase. *Salmonella* mutants lacking FraB are highly attenuated in mouse models of inflammation due to the toxic build-up of the substrate 6-phosphofructose-aspartate (6-P-F-Asp). This toxicity makes *Salmonella* FraB an appealing drug target, but there is currently little experimental information about its catalytic mechanism. Therefore, we sought to test our postulated mechanism for the FraB-catalyzed deglycation of 6-P-F-Asp (*via* an enaminol intermediate) to glucose-6-phosphate and aspartate. A FraB homodimer model generated by RosettaCM was used to build substrate-docked structures that, coupled with sequence alignment of FraB homologs, helped map a putative active site. Five candidate active-site residues—including three expected to participate in substrate binding—were mutated individually and characterized. Native mass spectrometry and ion mobility were used to assess collision cross sections and confirm that the quaternary structure of the mutants mirrored the wild type, and that there are two active sites/homodimer. Our biochemical studies revealed that FraB Glu214Ala, Glu214Asp, and His230Ala were inactive *in vitro*, consistent with deprotonated-Glu214 and protonated-His230 serving as a general base and a general acid, respectively. Glu214Ala or His230Ala introduced into the *Salmonella* chromosome by CRISPR/Cas9-mediated genome editing abolished growth on F-Asn. Results from our computational and experimental approaches shed light on the catalytic mechanism of *Salmonella* FraB and of phosphosugar deglycases in general.

Introduction

There are over 2600 serovars of *Salmonella enterica*, many of which are foodborne pathogens that cause an estimated 93 million human enteric infections and 155,000 cases of human diarrheal deaths each year [1−3]. Currently, there are no vaccines against the gastrointestinal serovars that are available for human use [4,5]. In addition, broad-spectrum antimicrobial therapy is disfavored because increased disruption of normal microbiota can exacerbate *Salmonella* infection as reflected in prolonged shedding of the organism in feces [6−8]. Identifying unique metabolic pathways, especially those that expose an Achilles' heel, would aid in design of *Salmonella*-specific antimicrobials. Such a prospect has emerged from the recent finding that *Salmonella* utilizes a naturally occurring Amadori compound, fructose−asparagine (F-Asn), as a carbon and nitrogen source [9,10], and that a blockade in the metabolism of F-Asn affords an opportunity for drug design.

F-Asn is formed by the non-enzymatic glycation reaction that couples the α-amino group of asparagine with glucose to culminate in a fructosamine after a spontaneous (Amadori) rearrangement [11]. F-Asn is present at wide-ranging concentrations in a variety of animal and human foods that we examined [12]. This observation lends support to the notion that *Salmonella* utilizes F-Asn as part of its nutrient repertoire in the animal gut.

The ability of *Salmonella* to utilize F-Asn is due to five horizontally acquired genes located in the *fra* locus: *fraR*, a transcriptional repressor of the GntR family, followed by a putative operon, which encodes an asparaginase (*fraE*), a transporter (*fraA*), a kinase (*fraD*), and a deglycase (*fraB*) (Fig. S1). We have recently validated the roles of these enzymes, and gained experimental support for a three-step catabolic pathway [10,13,14]. FraE, a periplasmic asparaginase, converts F-Asn to F-Asp [14]. Genetic studies [10] support the idea that FraA, a Dcu-type transporter, mediates transport of F-Asp from the periplasm to the cytoplasm. F-Asp is phosphorylated to 6-phosphofructose-aspartate (6-P-F-Asp) by the FraD kinase [13]. The FraB deglycase, the focus of this study, completes the pathway by converting 6-P-F-Asp to glucose-6-phosphate (G-6-P) and L-aspartate (L-Asp), central metabolic intermediates [10].

Salmonella mutants lacking *fraB* are highly attenuated in mouse models of *Salmonella*-induced inflammation due to the build-up of 6-P-F-Asp, the substrate of FraB and a toxic metabolic intermediate [10]; the basis for toxicity of this 6-phosphosugar is unclear, although parallels with other sugar phosphates that cause depletion of glycolytic intermediates [15] appear likely. This finding, together with the observation that only some members of the gut microbiome (e.g., Clostridia) are capable of utilizing F-Asn [16], motivated us to pursue *Salmonella* FraB as a drug target. Design and validation of potent FraB inhibitors require biochemical characterization of FraB and delineation of its catalytic mechanism, the goals of this study. Despite the long-standing

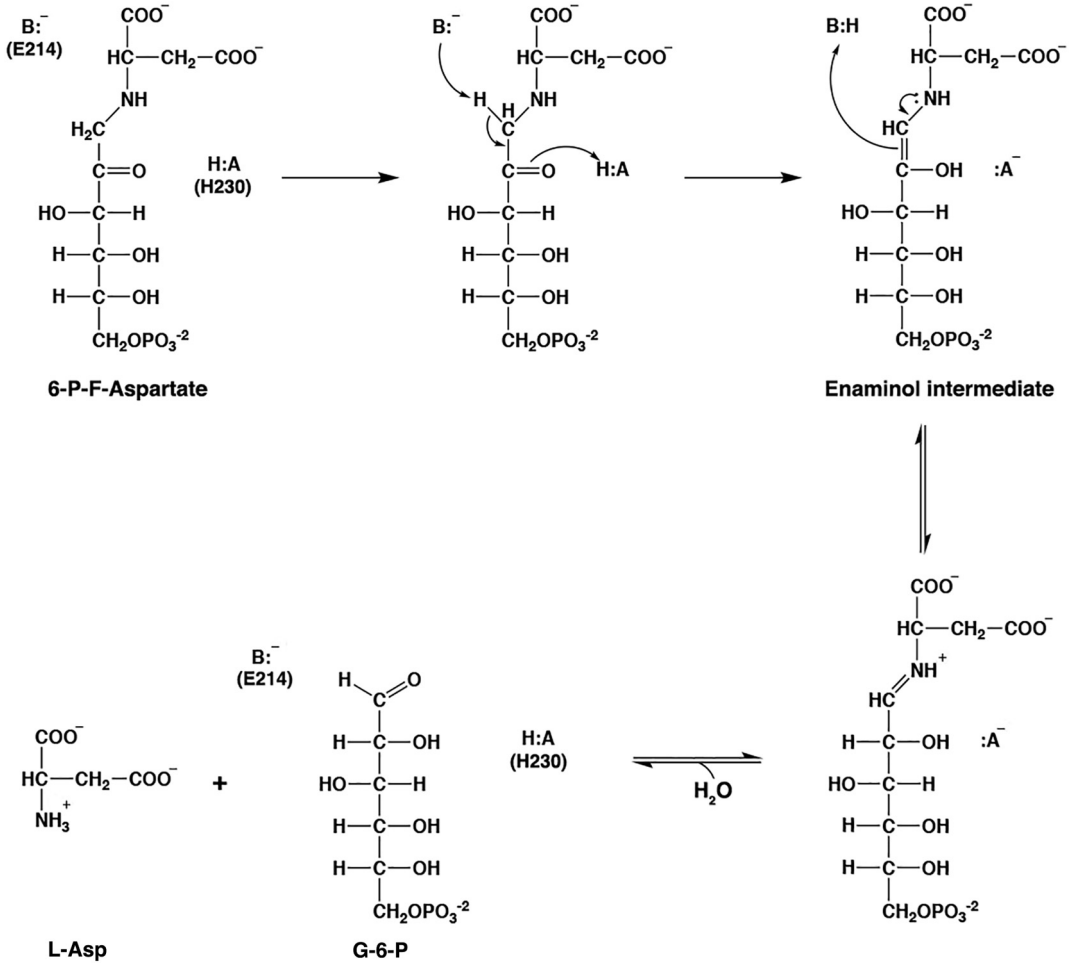

Fig. 1. A hypothetical catalytic mechanism for FraB. G-6-P, glucose-6-phosphate; L-Asp, L-asparate; 6-P-F-Asp, 6-phosphofructose-aspartate. This depiction does not include the initial ring-opening step, which converts the cyclical to the linear form.

recognition of microbial deglycases functioning in similar catabolic pathways that aid utilization of F-Lys, F-Val, or deoxyF-Gln [10,11,17–22], there is currently little information on the catalytic mechanism of these enzymes, a gap that we address here.

Based on phosphosugar isomerases, we postulated a mechanism that entails the use of a general acid and a general base to aid deglycation *via* an enaminol intermediate (Fig. 1). To validate the proposed mechanism, we employed an experimental approach that integrates computational modeling with substrate docking, kinetic studies on putative active-site mutants (informed also by an analysis of conserved residues), ion mobility (IM) and native mass spectrometry (MS) to validate structural and functional attributes, and finally genome editing and characterization of chromosomal *fraB* point mutants to cross-validate the *in vitro* findings. The collective picture that has emerged from these studies provides a platform for understanding the functioning of related deglycases that play a role in microbial metabolism of various Amadori compounds, and importantly offers a foundation for FraB-focused drug discovery efforts. Our roadmap for integrating analytical, biochemical, computational, and molecular biological methods to uncover the catalytic mechanism of an enzyme for which a structure is not available should be broadly applicable.

Results

Proposed mechanism for FraB catalysis

FraB converts 6-P-F-Asp to G-6-P and L-Asp. We have parsed the catalytic mechanism of FraB into two stages (Fig. 1): an initial isomerization followed by hydrolysis of a Schiff base. The homology-based identification of two sugar isomerase (SIS) domains in FraB (from residues 13–150 and 182–325; predicted by https://prosite.expasy.org/) suggested that FraB catalysis might parallel the mechanisms used by sugar isomerases. Our hypothetical scheme was inspired by in-depth studies of the glycolytic enzyme triose phosphate isomerase [23–26], where a general base (a deprotonated Glu) deprotonates the hydroxymethyl group in dihydroxyacetone phosphate to generate an enediol intermediate with electrophilic assistance from a general acid (a protonated His). The subsequent removal of a proton from this enediol by the same active-site histidine culminates in generation of glyceraldehyde-3-phosphate.

Mirroring the triose phosphate isomerase mechanism, we propose the involvement of general acid to lower the pK_a of one of the C1 hydrogens by polarizing the carbonyl at C2 (Fig. 1). We also postulate abstraction of one of the C1 hydrogens (*pro*-R?) by a general base to form an enaminol intermediate. Donation of a proton to the enaminol by the now protonated general base yields a Schiff base, which is then hydrolyzed to G-6-P and L-Asp. Because α/β-pyranose and α/β-furanose forms of fructose-amino acids are present in solution (with the β-pyranose being the predominant species) [27], ring opening of 6-P-F-Asp is essential prior to bond breakage. Because we have no information on whether the ring opening is enzyme assisted, we depict the mechanism beginning with the linear form.

Activity-pH profile of FraB

A rate-pH profile often provides experimental support to validate any proposed catalytic mechanism. Therefore, we tested the activity of FraB at different pH values ranging from 4.7 to 9.8 using acetate, Bis–Tris, HEPES, and CHES buffers. To exclude the possibility that FraB activity might be influenced by differences in buffer components, we included overlap points for correction (i.e., testing both acetate and Bis–Tris at pH 5.2, Bis–Tris and HEPES at pH 6.7, and HEPES and CHES at pH 8.5). We determined the initial velocities at different pH values and plotted the relative activity as a function of pH (Fig. 2). The bell-shaped pH-rate profile revealed an optimal pH between pH 7.7 to 8.5 (Fig. 2) and suggests that the catalytic mechanism of FraB requires participation of at least two titratable groups, possibly a general acid and a general base.

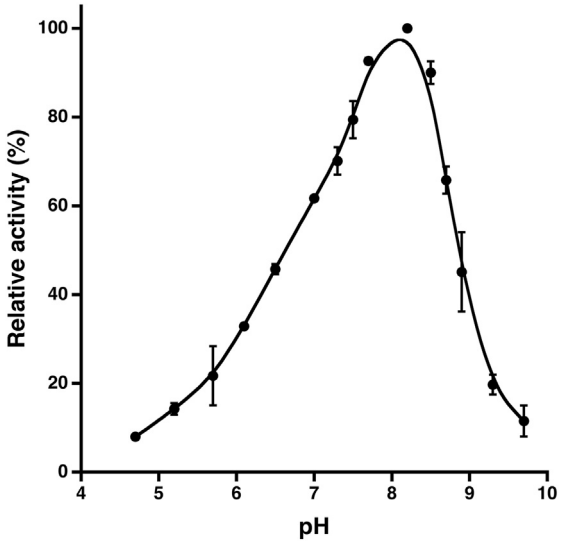

Fig. 2. The pH dependence of FraB activity. Relative activities were determined by using the FraB activity observed at pH 8.2 as 100%. The mean and standard deviation values were calculated from three independent experiments.

Homology modeling, docking, and MD simulation studies to identify the putative active site of FraB

Our initial objective was to conduct biochemical studies and interpret the results with a high-resolution structure. Despite our success in obtaining several milligrams of recombinant FraB and sustained efforts to obtain a crystal structure, this initiative was not fruitful. Therefore, we employed RosettaCM [28] to build a homology model of FraB using as templates 3FKJ and 3EUA (Fig. 3a and b), two bacterial phosphosugar isomerases with ~50% identity to FraB. This model was symmetrized and

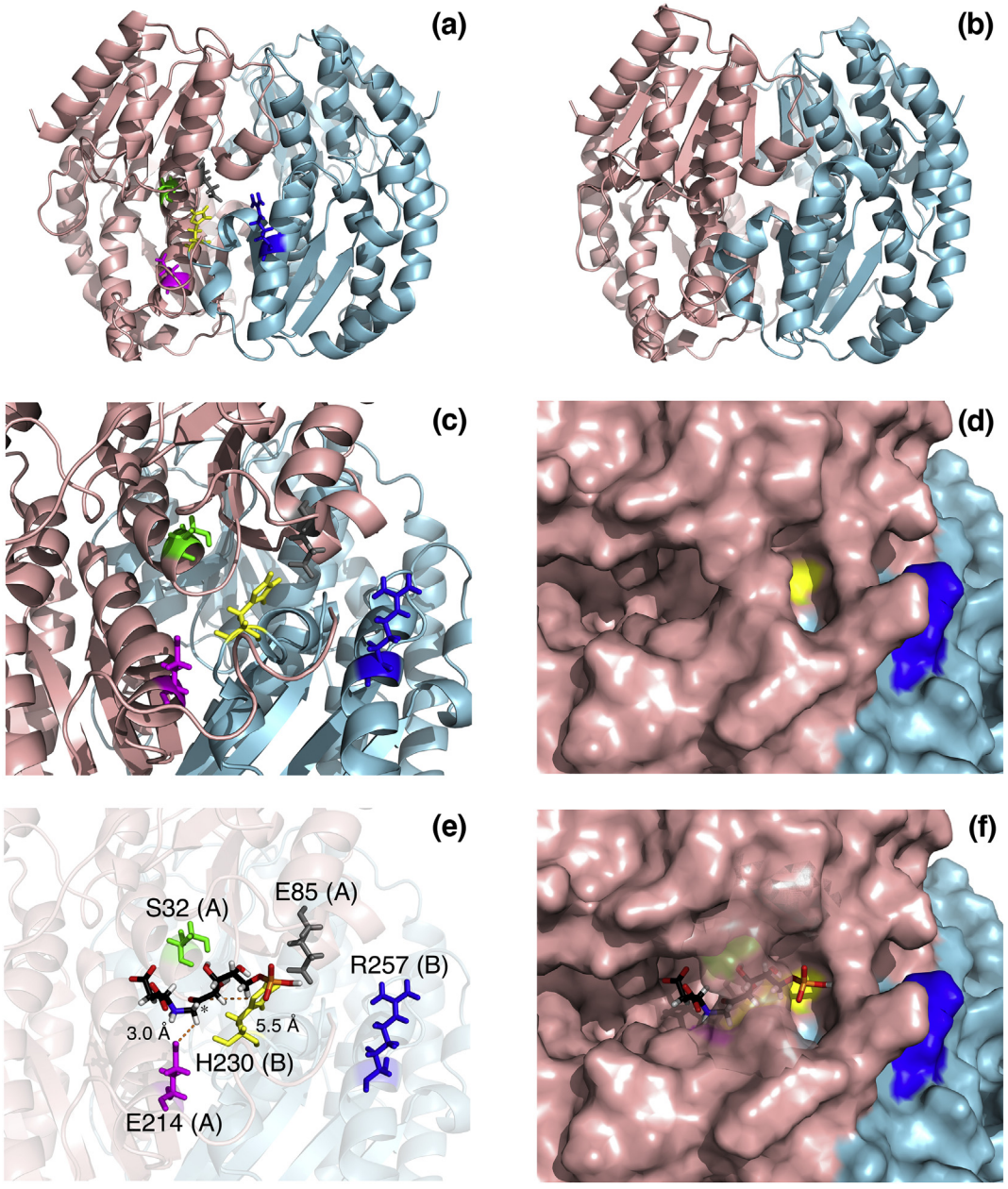

Fig. 3. Homology modeling of the FraB homodimer and docking of 6-P-F-Asp substrate in the putative active site. Coloring: chain A, light pink; chain B, light blue; residues: as indicated (S32, green; E85, gray; E214, magenta; H230, yellow; R257, blue). (a) Symmetrized homology model of FraB showing a side view of the binding pocket. (b) Crystal structure of *Salmonella* phosphosugar isomerase (3FKJ) used as one of the templates to generate the homology model. (c and d) Putative active site of FraB in cartoon and surface representation, respectively. (e and f) Close-up view of 6-P-F-Asp-bound FraB binding pocket in cartoon and surface representation, respectively. Views in panels e and f mirror panels c and d, respectively. Asterisk indicates the scissile bond.

relaxed in Rosetta for subsequent use in docking and simulations.

To derive experimental support for the FraB homodimer model (325-amino-acid residues/monomer), we used native MS, which transfers intact, native-like, kinetically-trapped protein complexes in solution to the gas phase. We also exploited native MS, in combination with dissociation and IM, for additional structural analysis of WT and mutant derivatives of FraB. First, we used native MS to estimate the K_D for FraB dimerization to be between 31 and 63 nM, indicating that the dimer is likely the biologically relevant oligomeric state for FraB (Fig. S2). Moreover, we determined that the dimer is the predominant form between pH 5 to 9 (Fig. S3), thus ruling out changes in the FraB oligomeric state as a reason for the sharp activity changes in this pH range. Second, ion mobiligrams from IM–MS experiments (Fig. S4) revealed the predominance of FraB dimers over the monomer and enabled calculations of the collision cross section (CCS; Fig. S5). IM is a gas-phase (electrophoresis-like) technique that passes ions through an electric field in a bath gas and enables measurements of rotationally averaged CCS values of proteins/protein complexes while also providing mass and charge information [29,30]. The average experimental CCS of FraB (3985 $Å^2$, in He) acquired from an RF-confining linear drift cell in He was compared with the theoretical CCS calculated for the RosettaCM-based FraB model. The experimental CCS was found to be in good agreement with the theoretical CCS: 0.9% higher than the CCS from the corrected projection approximation [31] (3950 $Å^2$, in He) and 7.9% lower than the CCS from projected superposition approximation [32] (4328 $Å^2$, in He). Finally, the FraB homology model, especially the dimer interface, was used to predict the surface-induced dissociation (SID) appearance energy that would be required to dissociate the FraB dimer. From energy-resolved MS plots, where the monomer formed over a range of SID collision energies is plotted, we determined an appearance energy of 540 eV (at a fragment intensity of 10%) that shows good agreement with the predicted value was 484 eV [33].

With a tertiary/quaternary structure model of FraB as well as a postulated mechanism, we sought to define a putative active site that could be experimentally validated. Sequence comparison of homologs often helps identify amino acid residues essential for structure and function. Therefore, we performed a ClustalW-based multiple sequence alignment of 50 FraB homologs (Fig. S6) and focused on highly conserved residues that are proximal in the homology model (Fig. 3c and d). In particular, we were interested in candidates for general acid (Cys, Glu, His) and general base (Glu, His) that could promote 6-P-F-Asp cleavage, and others that could engage in hydrogen-bonding (Ser, Thr) or electrostatic interactions (Arg, Lys) to promote 6-P-F-Asp binding. This exercise identified S32, E85, E214, H230, and R257 as candidates, which cluster together within a putative active-site cleft at the dimer interface (Fig. 3).

Next, we used GlideXP [34] to dock the linear form of 6-P-F-Asp into a FraB binding pocket that was identified by both SiteHound [35] and FTMap [36] (Fig. 3e and f). In one of the poses (Fig. 3), the docked ligand was proximal to S32, E85, E214, and H230. Moreover, in this pose, the phosphate in 6-P-F-Asp is near H230 as well as the N-terminal dipole end of the helix that starts with Pro84. When we performed a 100-ns molecular dynamics (MD) simulation, we also observed that S32, E85, E214, H230, and R257 were clustered together in the same pocket by the end of the simulation, indicating that R257 could move in to interact with the phosphate in 6-P-F-Asp (Supplementary Movie 1 shows the conformation before and after the MD simulation).

Based on the inter-atomic distances between specific side chains and the substrate functional groups, our expectation was that deprotonated-E214 and protonated-H230 could serve as the general base and acid, respectively, and that S32, E85, and R257 could support substrate binding. These residues are universally conserved among the FraB homologs that we examined (one exception: S32 is replaced by T32 in Clostridiales FraB; Fig. S6). Thus, based on the computational docking model and our postulated mechanism (informed in part by the rate–pH profile), we focused our first set of studies on five residues for site-directed mutagenesis: S32, E85, E214, H230, and R257. We report kinetic studies performed using the S32A, E85A, E214A, E214D, H230A, or R257A variants of FraB.

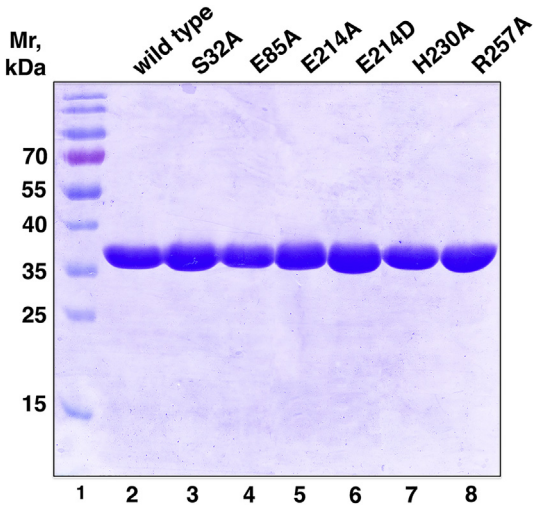

Fig. 4. SDS-PAGE [12% (w/v) polyacrylamide] analysis of recombinant FraB WT and mutant variants used in this study. Lane 1: Size marker. Lanes 2–8: Purified recombinant proteins (~6 μg protein in each lane).

Structural analyses of FraB wild type and its mutant derivatives

After overexpression in *Escherichia coli* and purification to near homogeneity following immobilized metal-affinity chromatography (IMAC; Fig. 4), ~15 mg of FraB wild type and six mutant derivatives (S32A, E85A, E214A, E214D, H230A, and R257A) were obtained from a 1-L *E. coli* culture. Using a high-resolution mass spectrometer, the mass of FraB wild type and its mutant derivatives was determined and found to be within ~0.01% of the predicted mass. While we used online buffer exchange coupled to ESI (with HCD) to obtain the mass of the homodimeric form of each variant (Table S1a), we used nano-ESI coupled to SID to cleave the native dimers and obtain the mass of the monomer form of each FraB variant (Table S1b).

To detect possible secondary structure changes induced by FraB mutations, we obtained the circular dichroism (CD) spectra of the six mutants and found that they matched the spectrum of the wild type (Fig. S7). Before proceeding with functional characterization of these mutants, we investigated if any of these mutations altered the quaternary (dimer) structure by using IM coupled to native MS. The traveling wave ion mobiligrams from IM–MS experiments (Fig. S4) show that all six mutants—S32A, E85A, E214A, E214D, H230A and R257A—exist predominantly as dimers, mirroring the findings with the wild type protein. The strong agreement in measured CCS values for FraB wild type and the mutant derivatives is consistent with all of them adopting the same overall fold. N_2 was used as the bath gas for the determination of CCS values of FraB wild type and mutant derivatives; these values agreed with the theoretical CCS values calculated in N_2 (Fig. S5).

Given the excellent agreement in data obtained by native MS and by alternative methods such as analytical ultracentrifugation, size-exclusion chromatography, and non-denaturing poly-acrylamide gel electrophoresis for many protein complexes over the past two decades [for example, see 37], the FraB homodimer identified by native MS is likely to be the functional form in solution. This contention is supported by our findings that (i) the dimer persists in native mass spectra over a broad pH and concentration range, (ii) WT and mutant dimers all have comparable CCS values, (iii) the experimentally determined CCS value of the WT dimer agrees with the value expected based on our computational model, and (iv) the SID appearance energy for dimer fragmentation is consistent with an equation that predicts appearance energy for dissociation consistent with inter- and intra-molecular bonding features of the dimer [33]. Despite possible limitations of native MS studies (e.g., gas phase measurement, instrument settings that might weaken the assembly, differences in ionization efficiency of different oligomeric states) [38], there is growing appreciation, however, that when ions are transferred into the gas phase—directly from solutions of appropriate ionic strength and pH—the solution structures are kinetically trapped for the short duration of the native MS experiment [30,39]. Consistent with this idea is our finding that native MS studies of FraB in the presence of the substrate could only detect the product-bound dimeric form indicating that the FraB dimer was active before and/or during electrospray (data not shown; see below for results with the E214A mutant).

Functional characterization of FraB wild type and its mutant derivatives

To gain insight into the functional role of each of the mutated residues in FraB catalysis, we determined the kinetic parameters for FraB (wild type) and six of its mutant derivatives (Table 1). Our K_m (116 μM), k_{cat} (63/min), and k_{cat}/K_m (5.4×10^5 M^{-1} min^{-1}) values for FraB wild type (Fig. 5A; Table 1) are similar to values reported for other deglycases: *E. coli* FrlB [22], which is specific for the ϵ-glycated 6-P-F-Lys (k_{cat}/K_m, 9.6×10^4 M^{-1} min^{-1}), and *Bacillus subtilis* YurP [21], which acts on α-glycated substrates (k_{cat}/K_m, 3.9×10^5 M^{-1} min^{-1} for 6-P-F-Val, its preferred substrate). *E. coli* FrlB and *B. subtilis* YurP share 27% and 43% amino acid identity, respectively, with *Salmonella* FraB.

Table 1. Comparison of kinetic parameters of FraB wild type and mutant derivatives

FraB variant	k_{cat} (min^{-1})	K_m (μM)	k_{cat}/K_m (M^{-1} min^{-1})	Relative k_{cat}/K_m (%)
Wild type	63 ± 10	116 ± 12	5.43×10^5	100
S32A	34 ± 1	3330 ± 150	1.02×10^4	~2
E85A	17 ± 1	1890 ± 450	0.74×10^4	~1
R257A	31 ± 2	2420 ± 180	1.27×10^4	~2
E214A	–	–	–	–
E214D	–	–	–	–
H230A	–	–	–	–

The mean and standard deviation values for k_{cat} and K_m were calculated from three independent experiments. No detectable activity is indicated by "–."

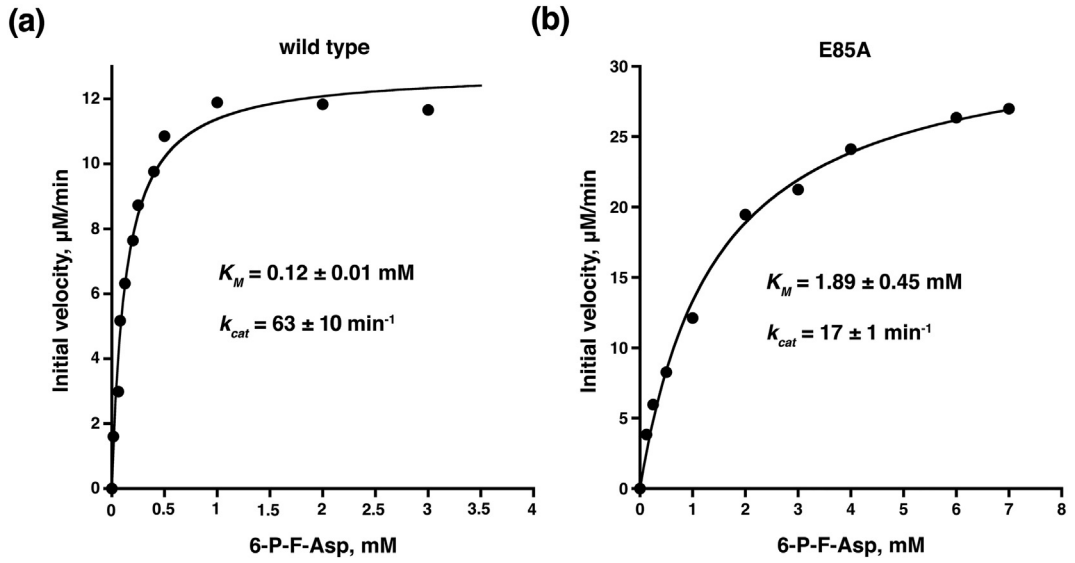

Fig. 5. Michaelis–Menten analysis of FraB wild type and the E85A mutant. While a representative plot is depicted, the values reported are the mean and standard deviation calculated from three independent experiments. See the Materials and Methods section for additional details on curve-fit errors.

The K_m increased by 29-, 16-, and 21-fold, respectively, with the S32A, E85A, and R257A FraB mutants compared to the wild type; the k_{cat} decreased by ~2- to 4-fold (Table 1, Figs. 5 and S8). Thus, S32, E85, and R257 appear to be involved in substrate binding. For E214A, E214D, and H230A, we could not observe any activity at pH 7.8 even using a 100-fold higher concentration of FraB. Based on the premise that protonated-H230 might serve as the general acid, we performed a "pH rescue" experiment. By lowering the assay pH from 7.8 to 5.5, we could restore the activity of H230A completely, confirming the role of H230 as a general acid (Fig. 6).

While all data point to the functioning of FraB as a dimer, we tested whether there are two active sites in

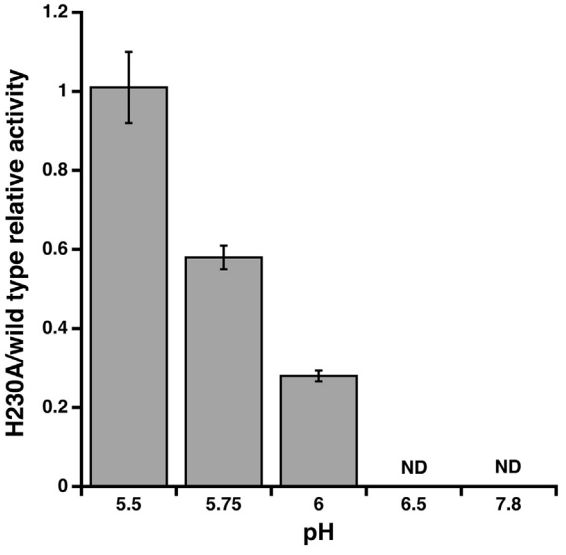

Fig. 6. Rescue of FraB H230A activity at low pH. The error bars represent the standard deviation of the mean determined from three independent experiments. ND, not detectable.

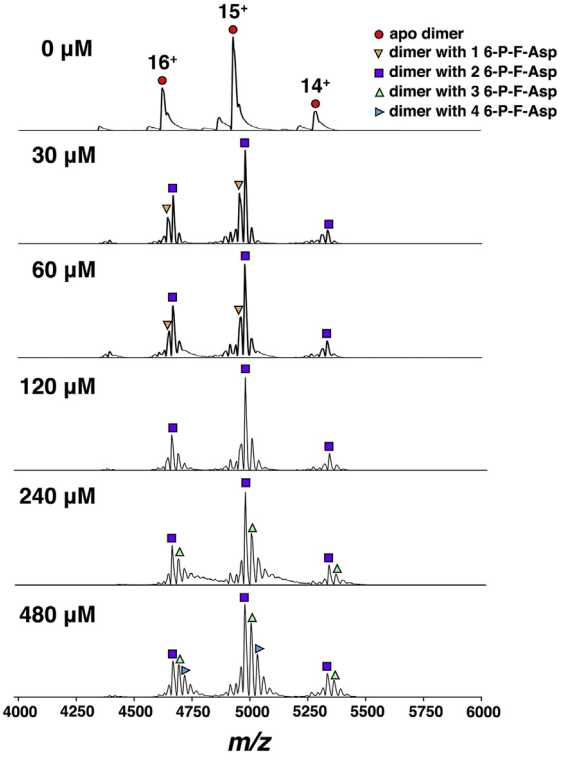

Fig. 7. Mass spectra of FraB E214A (3 µM) without or with indicated concentration of 6-P-F-Asp.

the dimer by exploiting the E214A mutant, which was catalytically inactive. Our expectation was that we should be able to determine the E-S stoichiometry if the E214A dimer could bind the 6-P-F-Asp substrate. Indeed, native MS studies revealed that E214A is able to bind (but not cleave) 6-P-F-Asp and retain two copies of the substrate/dimer. Upon titrating 30 to 240 μM 6-P-F-Asp to 3 μM FraB E214A, native MS revealed a mass consistent with two copies of the substrate/dimer (E_2S_2; Fig. 7). However, at >240 μM 6-P-F-Asp (>80-fold excess over substrate), we observed a small population of three and four substrate copies per FraB E214A dimer; the third and fourth copy appear to be due to non-specific binding, as the energy required to dissociate the third substrate copy from the E_2S_3 complex was lower compared to the second substrate from the E_2S_2 complex (data not shown).

Growth studies of *Salmonella fraB* point mutants

To understand the effect of *fraB* point mutations *in vivo*, growth of *Salmonella* wild type or E214A *fraB* or H230A *fraB* was assessed in media containing either 5 mM Glc or 5 mM F-Asn. *Salmonella* can utilize F-Asn as a carbon and nitrogen source [10]. The *fraB* mutations were introduced in the chromosome using λ red recombineering followed by selection for mutants using CRISPR/Cas9 targeting of the wild type *fraB* sequence. While all three strains grew equally well in 5 mM Glc as the sole carbon source (Fig. 8a), only the wild type grew on 5 mM F-Asn (Fig. 8b). Either E214A or H230A introduced in the *Salmonella* chromosome eliminates growth on F-Asn, confirming the essentiality of E214 and H230, and validating our *in vitro* kinetic data. Importantly, we could complement these growth defects by introducing the wild-type *fra* locus on a plasmid (Fig. 8b).

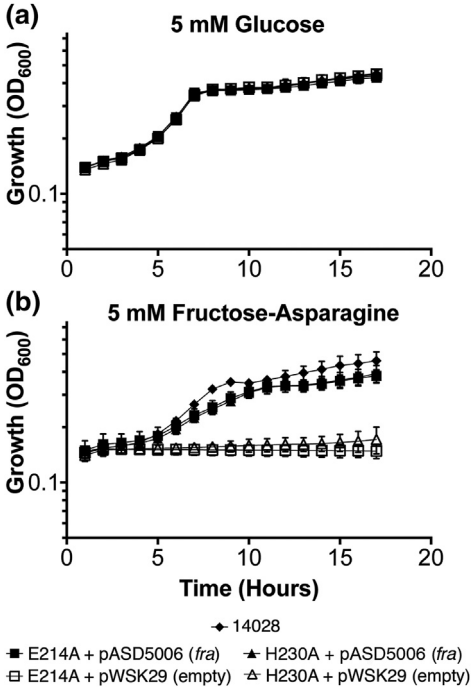

Fig. 8. Growth studies of *Salmonella* wild type and *fraB* point mutants on various carbon sources. *Salmonella* wild type (14028) and isogenic *fraB* point mutants were grown in M9 minimal media with ~19 mM ammonium chloride and supplemented with either 5 mM glucose (a) or 5 mM F-Asn (b). The *fra*B point mutants were complemented with either an empty vector (pWSK29) or a plasmid containing the entire *fra* island (pASD5006). The error bars represent standard deviation of the mean calculated from three biological replicates measured in triplicate (9 total data points).

Discussion

Results from our computational, biochemical, IM and native MS, and genetic studies further our understanding of the mechanism of the *Salmonella* FraB deglycase—the terminal enzyme in the pathway responsible for utilization of F-Asn by this bacterium. This advance, together with insights from the homology model of the FraB homodimer (with and without docked substrate), provides a foundation for *in silico* screening and for structure-based design of small-molecule inhibitors.

The microbial utilization of various fructosamines—a class of Amadori compounds—is well established [16–22]. While one route entails the use of oxidases [40,41], the other (relevant to this study) involves cleavage of the fructosamine between C1 of the sugar and the α-nitrogen of the amino acid [21,22]. The pioneering studies by Van Schaftingen and co-workers [20–22] provided the roadmap for understanding the pathway employed in the second route: transport of the fructosamine into the cell followed by phosphorylation and deglycation. Our scheme for the catalytic mechanism of FraB (Fig. 1) was inspired by these earlier studies where it was surmised from the reversibility of the FrlB deglycase that Schiff base formation and isomerization was the likely mechanism for the non-physiological condensation of G-6-P and lysine to form 6-P-F-Lys [20]. FrlB's hypothetical mechanism in turn was based on the precedent of glucosamine 6-phosphate synthase (GlmS) [42], which catalyzes the synthesis of glucosamine 6-phosphate (GlcN-6-P) from Fru-6-P and glutamine/ammonia (see below). Thus, an initial isomerization followed by Schiff base hydrolysis is one mechanistic path for the forward reaction of deglycases, an idea that we have validated here using FraB as the exemplar. While final support will await a high-resolution FraB structure, we have gained important insights by uncovering a suite of molecular determinants for substrate binding and cleavage by *Salmonella* FraB.

For the initial isomerization step catalyzed by FraB, the general base and general acid that support enaminol formation are likely E214 and H230, respectively. These two residues are essential for activity *in vitro* and *in vivo*; the latter finding was aided by our genome-editing experiments, which revealed that these individual *fraB* mutations in the *Salmonella* chromosome abolished the ability to grow on F-Asn (Fig. 8). In our substrate-docked model of FraB (Fig. 3), H230 is <5 Å from the C2 carbonyl oxygen in 6-P-F-Asp and E214 is <3 Å from the C1 *pro*-R hydrogen; these distances are consistent with our proposed mechanism for FraB. The need for such precise positioning is supported by our finding that even shortening of the side chain of E214 by a single methylene group is not tolerated as reflected in the complete loss of activity of E214D. This finding is not without precedent: the crystal structure of the yeast triose phosphate isomerase (TIM) E165D mutant showed that alterations in distance and orientation of the general base was the likely basis for the 1000-fold decreased TIMTIM activity of the mutant compared to the wild type [23].

In our postulated FraB catalytic mechanism, we do not know if the enzyme assists with ring opening. The crystal structure of the C-terminal isomerase domain of GlmS bound to the reaction product supported an isomerization mechanism in which an initial ring-opening by H504 is followed by a subsequent enolization by E488 [42]. Given the turnover rate of FraB is ~60 min^{-1} and the rate of spontaneous ring opening of Fru-6-P is ~1200 min^{-1} [43], ring opening (even if assisted by FraB) cannot be rate determining. We discuss two other observations pertinent to the FraB mechanism and the substrate-docked model. First, we considered that E85 might serve as either the general acid (instead of H230) or general base (instead of E214). However, a pH rescue experiment, similar to the one that completely recovered the activity of the H230A mutant (Fig. 6), left unchanged the pronounced k_{cat}/K_m defect of the E85A mutant at pH 5.5 (data not shown) and pH 7.5. Also, E214A, but not E85A, led to complete loss of activity *in vitro*, supporting the essentiality of E214 due to its role as a general base that aids enaminol formation. E85, however, might play a role in locking the position of the general acid through H-bonding as it is <2 Å from H230. Second, the individual mutagenesis of S32, E85, and R257 to alanine resulted in >20-fold increases in the K_m value relative to the wild type (Table 1). While S32 and E85 are well positioned (~3 Å) to engage in H-bonding with hydroxyl groups in 6-P-F-Asp, R257 is distant (~10 Å). However, our 100-ns MD simulation converges on structures that support a salt bridge between the phosphate in 6-P-F-Asp and R257 (Movie S1). K133 and R317 also seem positioned to interact with the two negatively charged carboxylates of 6-P-F-Asp, a testable postulate.

Our homology model of FraB illustrates the presence of two active sites/homodimer (Fig. 3), which we have now confirmed with the use of native MS (Fig. 7). Remarkably, each active site in the symmetric homodimer consists of residues drawn from both subunits (Fig. 3). One subunit contributes S32, E85, and E214, while the other provides H230 and R257. Akin to FraB, we find that the 16-aa spacing between the general base and general acid is maintained in *Salmonella* FrlB (E231 and H247; Bell, unpublished) and the C-terminal isomerase domain of GlmS (E488 and H504) [42]. We plan to undertake protein engineering initiatives to explore the significance of this conserved spacing for the catalytic mechanism of deglycases and sugar isomerases, and to better understand the unexpected interplay across the homodimeric interface in this enzyme superfamily.

Our work will aid drug discovery efforts that target *Salmonella* FraB. Although several members of the *Clostridia* class can also utilize F-Asn [16], these organisms are eliminated from the gut during *Salmonella*-mediated inflammation and F-Asn becomes exclusively accessible to *Salmonella* [44]. Moreover, because various foods contain appreciable levels of F-Asn [12], we have postulated that a FraB inhibitor in combination with dietary sources of F-Asn should be able to inhibit *Salmonella* growth *in vivo* [10,12,16]. While our ongoing high-throughput biochemical and *in silico* screenings are expected to identify non-covalent inhibitors of FraB, the active site that we have delineated here opens up possibilities for design of either dimerization inhibitors or "suicide substrate" ligands that mimic 6-P-F-Asp and have a "warhead" [45] to selectively inactivate *Salmonella* FraB by covalent modification of E214 and H230 in its intersubunit active site.

Materials and Methods

Computational modeling

RosettaCM-based homology model of FraB homodimer

Two homodimer templates with relatively high homology to *Salmonella* FraB were found in the protein databank: 3FKJ, putative phosphosugar isomerase from *Salmonella typhimurium*; 3EUA, putative phosphosugar isomerase from *B. subtilis*. These two templates had identities/similarities of 46/63% and 43/59%, respectively, to FraB. By assigning equal weight to both homologs, RosettaCM [28] was used to build 10,000 homology models of the FraB homodimer [46]. To select a single structure from the ensemble of 10,000 structures, a cluster

radius of 2 Å was used to group the models into four clusters. The largest cluster contained 84% of the structures, and importantly contained the best-scoring model. Since FraB contains two symmetric active sites, the best scoring model was symmetrized and relaxed in Rosetta for use in docking and MD.

Docking of substrate

The linear form of 6-P-F-Asp was prepared using Schrödinger's LigPrep [47]. Using Glide XP [34], 6-P-F-Asp was docked into a binding pocket (identified by SiteHound [35] and FTMap [36]) of the symmetrized homology model of FraB. In the docked pose shown in Fig. 3, the substrate is blanketed by S32, E85, E214, and H230 (see Discussion note concerning R257).

Molecular dynamics

Visual molecular dynamics (VMD) [48] was used to solvate the FraB homology model in a 14 Å-padded TIP3P water box. The solvated water box was then ionized using Na^+ and Cl^- ions at an ionic strength of 1 M. The system contained a total of 72,349 atoms. All simulations were run using NAMD 2.12 [49] and the CHARMM27 force field [50]. To prepare the system, two minimization and two equilibration stages were performed. In the first minimization stage, the ions and waters were minimized for 20,000 steps. In the second minimization stage, the entire system was minimized for 20,000 steps. In the first equilibration stage, the system was heated to a temperature of 300 K by systematically weakening the constraints. In the second equilibration stage, a 20-ps NPT simulation was performed. For the production run, a 100-ns NPT simulation was performed with periodic boundary conditions.

Biochemical studies of FraB

Site-directed mutagenesis of FraB

The FraB ORF was amplified by PCR with gene-specific primers using as template *Salmonella* genomic DNA. NcoI and EcoRI recognition sites were introduced in the forward and reverse PCR primers, respectively, to facilitate cloning into pET-33b (Novagen) to generate an N-terminal His_6-tag fusion followed by a tobacco etch virus (TEV) protease cleavage (Glu-Asn-Leu-Tyr-Phe-Gln) site. PCR-based mutagenesis was performed to generate FraB mutant derivatives using pET33b-FraB as the DNA template. For each mutant, a pair of forward and reverse primers was used (Table S2). The primers were first phosphorylated using T4 polynucleotide kinase (New England Biolabs), and PCR reactions were performed to amplify the entire plasmid. Each amplicon was then ligated using T4 DNA ligase to re-circularize the plasmid prior to transformation of *E. coli* DH5α cells. Following transformation, mini-prep plasmid DNAs, which had been isolated from individual colonies, were subjected to DNA sequencing at the Ohio State University (OSU) Genomics Shared Resource Facility to confirm that the entire FraB ORF was correct in each case. These mutant clones were then used to transform *E. coli* Rosetta (DE3) cells for overexpression of the desired FraB variant.

Overexpression and purification of FraB wild type and mutant derivatives

In all instances, a single bacterial colony was used to inoculate 2.5 mL of LB medium supplemented with 35 μg/mL kanamycin and 35 μg/mL chloramphenicol, and grown overnight at 37 °C with shaking. This saturated overnight culture was used to seed 250 mL of fresh LB medium containing the appropriate antibiotics. The cells were grown at 37 °C with shaking until OD_{600} ~ 0.6 and were then induced with 1 mM IPTG for 2 h. Following IPTG induction, the cells were harvested by centrifugation and the cell pellets were stored at −80 °C until further use.

Purification of FraB wild type and mutant derivatives was performed using IMAC. A 250-mL cell pellet obtained after overexpression was thawed on ice, re-suspended in 8 mL lysis buffer [90% buffer A (50 mM Tris−HCl, pH 7.5, 150 mM NaCl, 1 mM DTT); 10% buffer B (buffer A + 500 mM imidazole)] containing DNase I (40 U, Roche) and one cOmplete™ mini-protease inhibitor cocktail tablet (Roche), and sonicated (50% output power for 5 min, with cycles of 2 s on and 5 s off, Ultrasonic Processor, Cole-Parmer). After centrifugation of the crude lysate (24,000*g*, 30 min, 4 °C), the supernatant was applied to a 1-mL HisTrap column (GE Healthcare) that had been pre-equilibrated with 5 mL equilibration buffer (90% buffer A + 10% buffer B, without DTT). After washing the column with 10 mL of equilibration buffer, FraB was eluted using three successive elution steps: 7.5-mL gradient from 50 to 250 mM imidazole, 5-mL gradient from 250 to 500 mM imidazole, and 2.5 mL of 500 mM imidazole using an AKTA FPLC (GE Healthcare) purifier. After IMAC purification, fractions containing primarily FraB were (i) identified using SDS-PAGE and Coomassie Blue staining, (ii) pooled, and (iii) subjected to TEV digestion (TEV:-FraB, 1:20). TEV cleavage was effected during dialysis against 20 mM Tris−HCl (pH 7.5), 150 mM NaCl, and 1 mM DTT in two steps: 2 h at 22 °C, followed by 12−16 h at 4 °C.

The TEV cleavage reaction mixture was then bound to Ni^{2+}-charged cOmplete His-Tag

Purification Resin (Roche; binding capacity of 40 mg/mL of resin), which has been pre-washed thrice with ddH_2O and thrice with dialysis buffer (without DTT), to remove (i) His_6-tagged-TEV, (ii) uncleaved His_6-FraB, and (iii) the cleaved affinity tag. The supernatant was passed through a 0.22-μm Spin-X filter (Sigma, CLS8160) and the purity of the flow-through, which contains FraB without the affinity tag, was assessed by SDS-PAGE (Fig. 4). The molecular mass was confirmed by ESI−MS analysis (Table S1). The concentration of each FraB variant was determined using the molar extinction coefficient (50,390 M^{-1} cm^{-1}) at 280 nm, and the final preparations [in 10% (*v*/v) glycerol] were stored at −80 °C in small aliquots for subsequent biochemical enzyme assays.

CD spectroscopic analysis of FraB wild type and mutant derivatives

The purified FraB wild type and mutant stocks were dialyzed against 25 mM sodium phosphate (pH 7.5) and diluted to obtain 10 μM samples. The CD spectra of these protein samples were obtained in a Jasco spectropolarimeter using a quartz cuvette of 1-mm path length. Measurements were taken between 195 and 260 nm, and three scans were averaged to obtain the final spectrum in each instance. For each protein, the final spectrum was obtained by subtracting the buffer spectrum from that of the protein. The final data are expressed in molar ellipticity (Fig. S7).

FraB activity assay

FraB assays were performed essentially as described earlier [10,14,16] and carried out at 37 °C in a 30-μL total reaction volume. 6-P-F-Asp was synthesized as described before [51] and was a kind gift from Prof. E. J. Behrman (OSU). Since the FraB reaction generates G-6-P, we employed a glucose-6-phosphate dehydrogenase (G6PD; Sigma G6378)-based coupled enzyme assay. The continuous measurement of NADPH produced by G6PD was taken as a direct readout of the G-6-P produced by FraB. Typically, our assays entailed a 27-μL reaction mix containing 25 mM HEPES (pH 7.5), 5 mM $MgCl_2$, 0.1 mM EGTA, and 0.5 mM $NADP^+$ with a defined concentration of 6-P-F-Asp, which was first incubated at 37 °C for 3 min. To this mixture was added in tandem 1.5 μL FraB (0.3 μM recombinant FraB) and 1.5 μL G6PD (0.075 U/ μL), each of which had been pre-incubated separately at 37 °C for 3 min. Note that the Mg^{2+} included in our assay is to support G6PD not FraB activity; it is well known that phosphosugar isomerases are metal independent unlike sugar isomerases [39].

From the 30-μL reaction that was assembled and initiated, 28-μL was immediately transferred to a 384-well microplate and the absorbance at 340 nm was monitored continuously using a SpectraMax M5 Microplate Reader (Molecular Devices; integration time of 1000 ms; settle time of 300 ms) that facilitated continuous spectrophotometric readout. Linear regression analysis of NADPH generated as a function of time was used to calculate the initial velocity ($0.97 \leq r^2 \leq 0.99$). For each assay, a control was performed that included all assay components except the FraB wild type (or its mutant derivatives) in order to account for any residual G-6-P in the substrate.

For the rate-pH profile and for the rescue assays, activity was measured using 1 mM 6-P-F-Asp. We used as buffer acetate for pH 4.7 to 5.2, Bis−Tris for pH 5.2 to 6.7, and HEPES for pH 6.7 to 8.5, and CHES for 8.5 to 9.8. For the pH-rate profile, we typically used 0.3 μM FraB in our assays. Given the decreased activity at low pH values, we used 0.5 to 1 μM FraB WT in the low pH rescue assays in order to obtain reliable initial velocity measurements; for the H230A mutant, we used 2.8 μM at pH 6 and 0.93 μM at pH 5.5 and 5.75. Since we detect FraB activity using a G6PD-based coupled assay, we tested the activity of *Saccharomyces cerevisiae* G6PD (Sigma) between pH 9.0 to 5.3 using 100 μM G-6-P as the substrate. While we found that G6PD exhibits a 3- to 5-fold decrease in its optimal activity at pH 9.0 and 5.3, respectively (not shown), this decrease is unlikely to influence the outcome of the FraB coupled assay given the vast excess of G6PD that was used (0.11 U/30 μL). This amount of G6PD is sufficient to convert G-6-P that might result even from near-complete utilization of 1 mM 6-P-F-Asp in the FraB assay conducted at pH 5.3. However, the time courses that we used typically only resulted in consumption of <5% of the starting substrate amount (1 mM), thus ensuring that G6PD is never limiting.

To determine the Michaelis−Menten kinetic parameters of FraB, assays were performed at varying 6-P-F-Asp concentrations (15 μM to 3.5 mM) using 0.3 μM FraB. For S32A, E85A, and R257A, we used 0.125 mM to 8 mM 6-P-F-Asp; we used 0.7 μM enzyme for S32A and R257A, and 2 μM for E85A to compensate for its weaker activity. To calculate the k_{cat} and K_m, the initial velocity determined at each substrate concentration was subject to the Michaelis−Menten curve-fitting option in Kaleidagraph (Synergy Software). The curve-fit errors for K_m and k_{cat} did not exceed 26% and 7%, respectively, with $r^2 \geq 0.97$ in all instances. As E214A, E214D, and H230A were practically inactive at pH 7.7, Michaelis−Menten analyses could not be performed with these mutant derivatives.

Native MS studies

Sample preparation

FraB wild type and mutant derivatives were buffer exchanged into 100 mM ammonium acetate (Sigma-Aldrich, St. Louis, MO) using 6-kDa cutoff Micro Bio-Spin 6 Columns (Bio-Rad, Hercules, CA). A NanoDrop spectrophotometer (Thermo Scientific) was used to measure the protein concentration using absorbance at 280 nm. The protein solutions were then diluted to desired concentrations with 100 mM ammonium acetate. For the pH titration experiments, acetic acid and ammonia solution were used to obtain the desired pH between 5 and 9 (Fig. S3). FraB wild type protein was buffer exchanged into 100 mM ammonium acetate and then diluted to 100 nM using solutions of different pH. For FraB-ligand complex characterization, 6-P-F-Asp was diluted using 100 mM ammonium acetate to the desired concentration and then mixed with protein at the indicated ratios at 25 °C. The samples were kept on ice (typically for <60 s), while the capillary tip was being prepared and sprayed soon after.

Orbitrap

Experiments to determine the exact mass of FraB, the approximate K_D for dimerization of FraB, and FraB-substrate stoichiometry were conducted using an in-house modified Exactive Plus EMR mass spectrometer (Thermo Scientific), whose transfer multipole was replaced by a selection quadrupole and which had a customized SID device installed between the selection quadruple and the C-trap [52]. Except for exact mass determination, all experiments were performed in transfer mode, with the voltages on SID lenses adjusted to transmit the ions without surface collisions.

A nano-electrospray ionization (nano-ESI) source was used on the modified Exactive Plus EMR. Borosilicate glass capillaries (34507−99, Kimble) were pulled with a P-97 micropipette capillary puller (Sutter Instruments). Protein samples were introduced by applying a 1.1−1.3 kV voltage to a platinum wire inserted into the back of the glass capillaries after they were filled with 5 μL FraB protein solution. The following instrument parameters were used: capillary temperature 125 °C, sheath gas flow rate 0, S-lens RF level 200. For all experiments on the modified Exactive Plus EMR, the maximum injection time was set to 200 ms and resolution was set to 8750. Mass spectra were extracted with Xcalibur 2.2 (Thermo Scientific) and processed with UniDec Launcher Version 2.6.5 [53].

For determining (i) the approximate K_D for dimerization of FraB (Fig. S2), (ii) the effect of pH on the oligomeric state (Fig. S3), and (iii) FraB-substrate stoichiometry (Fig. 7), HCD 20 V was used for clean-up. For exact mass determination (Table S1), both dimer and monomer masses were determined. For SID to produce de-adducted monomers, HCD 1 V was used, and an SID voltage of 165 V was applied for dissociation of the dimer. The resulting monomer was used to calculate the exact monomer mass. In the SID experiments, the potentials were applied on lenses on the SID device to guide the ions to collide with the surface while other electrodes were tuned to maximize the transmission of fragment ions. For exact mass determination of dimers, an online protein buffer-exchange system was constructed with an in house-packed size exclusion chromatography column using materials from a 6-kDa cutoff Micro Bio-Spin 6 Column (Bio-Rad, Hercules, CA) connected to an Ultimate 3000 RSLC liquid chromatography system (Thermo Scientific). The online protein buffer-exchange system was coupled to the Exactive Plus EMR (https://doi.org/10.26434/chemrxiv.8792177.v2). Three to five μL (~12 to 90 μM, based on the stock) of FraB solution was injected into the system manually by syringe. Ammonium acetate (200 mM) was used as the mobile phase at a flow rate of 100 μL/min. A heated electrospray ionization source was used with the following instrumental parameters: spray voltage, 4 kV; capillary temperature, 320 °C; sheath gas flow rate, 50; S-lens RF level, 200; and HCD, 200 V. For the pH study, 10 μL aliquots of 100 nM FraB at different pH values were stored in a 96-well plate (Thermo Scientific, Loughbrough, UK) and placed in the Advion TriVersa NanoMate (Advion Biosciences, Ithaca, NY). Samples were then injected into the mass spectrometer using the NanoMate nano-electrospray device at a spray voltage of 1.50 kV and gas pressure of 0.30 psi.

To determine the energy required to dissociate the substrate from the E214A FraB dimer−substrate complex, E214A FraB (6 μM) was mixed with 6-F-Asp (50 μM) and introduced into the modified Exactive Plus EMR with the maximum injection time set to 2000 ms. A series of HCD energies from 5 to 200 V (collision energy is $\Delta V \times$ the charge state of the precursor) was applied to the isolated E214A FraB-substrate complexes: E214A FraB dimer with one, two, or three 6-P-F-Asp copies. The HCD energy to produce the same intensity of E214A FraB with n 6-P-F-Asp and FraB with $(n-1)$ 6-P-F-Asp was determined as the dissociation energy for the n^{th} 6-P-F-Asp.

Q-IM-TOF

Experiments to determine the oligomeric state of FraB as well as traveling wave ion mobility (TWIM)-based CCS values were conducted on a Q-IM-TOF

instrument (Synapt G2, Waters Corporation, Manchester, UK) modified in-house to include a customized SID device installed between the trap cell and the IM cell [54]. All experiments were performed in transfer mode, in which the voltages on SID lenses were adjusted to transmit the ions without surface collisions. Nano-ESI was used to introduce protein samples by applying 1.2−1.3 kV voltage to a platinum wire inserted into the glass capillaries already filled with 5 μL of 7 μM FraB. The following instrument parameters were used: sampling cone voltage, 20 V; extraction cone voltage, 1 V; source temperature, 20 °C; backing pressure, 3.2 mbar; trap gas flow, 2 mL/min; helium cell gas flow, 120 mL/min; IMS gas (N_2) flow, 60 mL/min; trap DC entrance, 0 V; trap DC bias, 45 V; trap DC 2 V; trap DC exit, 0 V; trap wave velocity, 250 m/s; trap wave height, 4 V; IMS DC entrance, 15 V; helium cell DC, 25 V; helium exit, −5 V; IMS DC bias, 3 V; IMS DC exit, 0 V; IMS wave velocity, 320 m/s; IMS wave height, 20 V; transfer DC entrance, 5 V; transfer DC exit, 10 V; transfer wave velocity, 65 m/s; and transfer wave height, 2 V. All mass spectra were processed with MassLynx v4.1 and DriftScope v2.1 (Waters Corporation, Manchester, UK).

Experiments to determine FraB CCS values with an RF-confining linear drift cell were conducted on an in-house modified Q-IM-TOF instrument (Synapt G2, Waters Corporation, Manchester, U.K.) with the TWIM cell replaced by the 25.2-cm-long drift cell. Voltages within the drift cell and surrounding ion optics were optimized to decrease ion activation while maintaining the ion intensity for sensitive detection. Briefly, the potential bias was adjusted along the length of the drift cell for 10 drift voltages spanning the range of 163−252 V. Helium gas was set at a flow rate of 160 mL/min to provide a pressure of ~2.2 Torr within the cell. Drift times for each drift voltage were plotted as a function of pressure/drift voltage to provide a mobility value corrected for standard pressure and temperature. Since the RF-confining drift cell does not require the calibration procedure that is essential for TWIM experiments, it provides CCS values based on first principles. The experimental CCS was calculated using methods reported previously [55,56].

The experimental CCS values for FraB wild-type and mutants measured with TWIM were determined as described before [57]. The CCS calibrants were β-lactoglobulin dimer (charge states +11 to +13), transthyretin tetramer (charge states +14 to +16), avidin tetramer (charge states +15 to +18), concanavalin A tetramer (charge states +20 to +22) and serum amyloid P pentamer (charge states +23 to +26). While serum amyloid P was purchased from Millipore (Burlington, MA), the remaining protein standards were purchased from Sigma-Aldrich (St. Louis, MO). These standards were prepared at 10−20 μM in 100 mM ammonium acetate.

Determination of the theoretical collisional cross-section values of FraB wild type and its mutant derivatives

The theoretical CCS values were calculated from our RosettaCM-generated homodimer structure using the projection approximation (PA) model [31] and the projection superposition approximation (PSA) model [32]. IMPACT [58] (impact.chem.ox.ac.uk) was used for the PA model calculations. The PA model typically underestimates the CCS of protein complexes by 14% [59], so a scaled PA method [60] was applied. The PSA Web Server (psa.chem.fsu.edu) was used for the PSA model [31]. The theoretical CCS calculation was performed in both He and N_2, with the gas radius set to 1.2 and 1.5 Å respectively [61].

Generation of FraB point mutants by CRISPR−cas9 mediated genome editing

Bacterial strains and growth media

All bacterial strains used are listed in Table S3. Bacterial strains were grown in Luria−Bertani (LB) broth, or minimal M9 media containing the following [62]: 1× M9 salts, 2 mM $MgSO_4$, 0.1 mM $CaCl_2$, 0.01 mM thiamine, and trace metals [63]. As appropriate, these were supplemented with antibiotics including spectinomycin (spec) and chloramphenicol (cam) at 100 and 30 μg/mL respectively, or anhydrotetracycline (atet) at 100 ng/mL. For *in vivo* growth curves, data points were collected using SpectraMax M5 that monitored OD_{600} for 17 h at 37 °C.

Electroporation

E. coli and *Salmonella* strains were made electrocompetent using the mannitol/glycerol protocol [64] and electroporated using 2-mm gap cuvettes (Molecular BioProducts) with settings of 25 μF, 400 Ohms, and 2.5 kV in an electroporator (BTX ECM630). Before plating, post-electroporation recovery entailed growth for 1 h in 1 mL of LB at either 30° or 37 °C (depending on the strain).

Generation of chromosomal FraB point mutants

To generate *fraB* E214A or *fraB* H230A point mutations in the chromosome, we used the no-SCAR (Scarless Cas9 Assisted Recombineering) method that exploits the lambda Red recombinase and CRISPR/Cas9 [65]. First, the 20-bp *ack* sgRNA-encoding region of pKDsgRNA-*ack* [65] was

replaced with that encoding a 20-bp *fraB* sgRNA (one each for E214A and H230A). This objective was accomplished by PCR-mediated amplification of the two halves of the pKDsgRNA-*ack* minus the *ack* sgRNA-encoding sequence; by including in one of the two PCR primers 20-bp of the appropriate *fraB* sequence, we exploited In-fusion (Clontech)-mediated recombineering to recircularize and yield pKDsgRNA-fraB.

Two *fraB* sgRNA plasmids were needed since the two mutations we sought to engineer did not fall within a 20-bp segment. The primer pairs used to generate the two halves of the sgRNA plasmid that was required to create the E214A mutation were BA3304/BA3305 and BA3306/BA3307, and that for the H230A mutation were BA3374/BA3305 and BA3375/BA3307 (Table S2). The PCRs to generate the two halves was performed using Clontech HiFi polymerase mix. The PCR amplicons were gel purified (Qiagen) and combined in an HD In-fusion reaction (Clontech). Chemically competent Stellar cells (Clontech) were mixed with 2 μL of the HD In-fusion reaction, plated on LB spec, and incubated overnight at 30 °C. Transformants were screened by colony PCR using Taq DNA polymerase (NEB) and the primer set BA3308/BA3309, which was designed to amplify the sgRNA region of pKDsgRNA plasmids. Colonies that yielded the correct-size PCR amplicons were grown in LB spec at 30 °C overnight and subsequently used to obtain plasmid minipreps (Qiagen). These purified plasmids were sent for DNA sequencing at the OSU Plant Microbe Genomics Facility, and sequencing was performed with primer BA3310 to identify the positive clones. We named the plasmids thus obtained as pASD1301 (E214A) and pASD1316 (H230A) (Table S3).

S. enterica strain ATCC 14028 was electroporated with plasmid pCas9-CR4. The resulting strain, which was named ASD1300, was then electroporated with pASD1301 or pASD1316, yielding strains that we labeled ASD1301 or ASD1318, respectively. ASD1301 or ASD1318 were used to create the E214A or H230A mutations in the chromosome, respectively.

Lambda Red mutagenesis was used to introduce the *fraB* point mutations into the chromosome. ASD1301 or ASD1318 were grown in 4 mL of SOC media at 30 °C overnight. The next day, the overnight culture was diluted 1:100 in SOC cam spec and grown at 30 °C for three to 4 h, prior to induction of lambda Red with 50 mM arabinose for 20 min. The cells were then electroporated with 10 μM 70-bp double-stranded DNA that encodes the mutation of interest. The double-stranded DNA was prepared by mixing two complementary single-stranded oligonucleotides, incubating at 98 °C for 10 min, and annealing at room temperature (Table S3). After post-electroporation recovery in 1 mL of SOC media for 1.5 h, the transformation reaction was serially diluted, plated separately on LB cam spec and LB cam spec atet, and incubated at 30 °C overnight. The *fraB* regions from the colonies on the LB cam spec atet plates were amplified by PCR with primers BA3368 and BA3369 for E214A or BA2701/BA2702 for H230A. The PCR products were sent for DNA sequencing at the OSU Plant Microbe Genomics Facility, and those that were found to contain the desired mutation were stored for further use. The guide RNA plasmids, pASD1301 and pASD1316, from strains ASD1301 and ASD1318, respectively, were cured by streaking confirmed mutants on LB cam plates and incubating at 40 °C overnight. This curing generated strains ASD1307 and ASD1339.

Curing pCas9-CR4

Curing of pCas9-CR4 was accomplished using another plasmid that encodes an sgRNA against the p15A origin of pCas9-CR4 [65]. ASD1307 and ASD1339 were electroporated with pKDsgRNA-p15 and plated on LB spec plates at 30 °C overnight. Colonies were re-streaked on LB spec atet at 30 °C overnight. Colonies were then re-streaked on LB and incubated at 40 °C; since pKDsgRNA-p15 has a temperature-sensitive replicon, the shift to higher temperature helps cure this plasmid. Colonies of each of strain were then patched on LB, LB cam, and LB spec at 37 °C. All colonies patched were cam sensitive and spec sensitive, indicating that pCAS9-CR4 and pKDsgRNA-p15 were cured. These new strains were designated as ASD1312 and ASD1355 (Table S3).

Complementation of point mutants

Each point mutant strain (ASD1312 or ASD1355) was electroporated as described above with the *fra* island complementation plasmid, pASD5006, that was previously published [9] or with pWSK29 as an empty vector control. All strains were assayed in growth curves with either 5 mM glucose or 5 mM F-Asn as described above, and compared to the wild type strain 14028 (Fig. 8).

Note on FraB sequence numbering

When we initiated these studies on FraB, we relied on an annotation that resulted in a 331-amino-acid ORF. Subsequent informatics revealed that Met7 (and not Met1) was the likely initiator, and that FraB *in vivo* is likely to be only 325 amino acids. Indeed, a proteomics study [66] confirmed this expectation. However, since most of the biochemical studies had been completed when we made this discovery pertaining to the N-terminal addition of six amino acid residues, we report here the activity of the variants that contain the six additional residues. We

performed a control experiment wherein we compared the activity of the 325- and 331-amino-acid FraB wild type variants, and found that their activity is the same within experimental error. For simplicity, all of the numbering used in this study corresponds to the 325-amino-acid variant (Fig. S6).

Supplementary data to this article can be found online at https://doi.org/10.1016/j.jmb.2019.08.017.

Acknowledgments

We are grateful to Prof. Edward J Behrman and Alex Bogard (OSU) for the generous gift of fructose−asparagine and 6-phosphofructose-aspartate, and to Mikayla Borton (laboratory of Dr. Kelly Wrighton, Colorado State University) for kindly providing sequences of the bacterial FraB homologs. We thank Alyssa Stiving (OSU) for the linear drift tube CCS measurement and calculation, and Dr. Craig McElroy, Director, Instrumentation, OSU College of Pharmacy, for his kind assistance with instrument training. This work was supported by the National Institutes of Health (R01-AI116119 to B.A., V.W., and V.G., and R01-AI140541 to B.A., C.E.B., S.L., and V.G.).

Received 1 April 2019;
Received in revised form 27 August 2019;
Accepted 28 August 2019
Available online 4 September 2019

Keywords:
enzyme mechanism;
deglycase;
Amadori products;
Salmonella

† Current addresses: A. Sengupta, Sygnature Discovery, Nottingham, NG1 1GR, United Kingdom.

§ Current addresses: J. Wu, Regeneron Pharmaceuticals, Tarrytown, New York, NY 10591, USA.

¶ Current addresses: T.-H. Chen, New England Biolabs, Ipswich, MA 01938, USA.

‡ These authors contributed equally to this work.

Abbreviations used:
F-Asn, fructose−asparagine; G-6-P, glucose-6-phosphate; L-Asp, L-aspartate; MS, mass spectrometry; IM, ion mobility; CCS, collision cross section; SID, surface-induced dissociation; MD, molecular dynamics; IMAC, immobilized metal-affinity chromatography; CD, circular dichroism; GlmS, glucosamine 6-phosphate synthase; TEV, tobacco etch virus; OSU, Ohio State University; G6PD, glucose-6-phosphate dehydrogenase; TWIM, traveling wave ion mobility.

References

[1] J.C. Buzby, T. Roberts, The economics of enteric infections: human foodborne disease costs, Gastroenterology. 136 (2009) 1851−1862.
[2] Kirk MD, Pires SM, Black RE, Caipo M, Crump JA, Devleesschauwer B, et al.: World Health Organization estimates of the global and regional disease burden of 22 foodborne bacterial, protozoal, and viral diseases, 2010: a data synthesis. PLoS Med. 2015;12.
[3] S.E. Majowicz, J. Musto, E. Scallan, F.J. Angulo, M. Kirk, S.J. O'Brien, et al., The global burden of nontyphoidal Salmonella gastroenteritis, Clin. Infect. Dis. 50 (2010) 882−889.
[4] L.B. Martin, Vaccines for typhoid fever and other salmonelloses, Curr. Opin. Infect. Dis. 25 (2012) 489−499.
[5] R.A. Strugnell, T.A. Scott, N. Wang, C.Y. Yang, N. Peres, S. Bedoui, et al., Salmonella vaccines: lessons from the mouse model or bad teaching? Curr. Opin. Microbiol. 17 (2014) 99−105.
[6] M. Diard, M.E. Sellin, T. Dolowschiak, M. Arnoldini, M. Ackermann, W.D. Hardt, Antibiotic treatment selects for cooperative virulence of Salmonella typhimurium, Curr. Biol. 24 (2014) 2000−2005.
[7] S. Gopinath, J.S. Lichtman, D.M. Bouley, J.E. Elias, D.M. Monack, Role of disease-associated tolerance in infectious superspreaders, Proc. Natl. Acad. Sci. U. S. A. 111 (2014) 15780−15785.
[8] J. Wistrom, M. Jertborn, E. Ekwall, K. Norlin, B. Soderquist, A. Stromberg, et al., Empiric treatment of acute diarrheal disease with norfloxacin. A randomized, placebo-controlled study. Swedish Study Group, Ann. Intern. Med. 117 (1992) 202−208.
[9] Ali MM, Newsom DL, Gonzalez JF, Sabag-Daigle A, Stahl C, Steidley B, et al. Fructose−asparagine is a primary nutrient during growth of Salmonella in the inflamed intestine. PLoS Pathog. 2014;10:e1004209.
[10] A. Sabag-Daigle, H.M. Blunk, A. Sengupta, J.K. Wu, A.J. Bogard, M.M. Ali, et al., A metabolic intermediate of the fructose−asparagine utilization pathway inhibits growth of a Salmonella fraB mutant, Sci Rep-Uk. 6 (2016) 28117.
[11] V.V. Mossine, T.P. Mawhinney, 1-Amino-1-deoxy-D-fructose ("fructosamine") and its derivatives, Adv Carbohyd Chem Bi. 64 (2010) 291−402.
[12] J. Wu, A. Sabag-Daigle, Metz TO, B.L. Deatherage Kaiser, V. Gopalan, E.J. Behrman, et al., Measurement of fructose−asparagine concentrations in human and animal foods, J. Agric. Food Chem. 66 (2018) 212−217.
[13] P.K. Biswas, E.J. Behrman, V. Gopalan, Characterization of a Salmonella sugar kinase essential for the utilization of fructose−asparagine, Biochem. Cell Biol. 95 (2017) 304−309.
[14] A. Sabag-Daigle, A. Sengupta, H.M. Blunk, P.K. Biswas, M.C. Cron, A.J. Bogard, et al., Salmonella FraE, an

asparaginase homolog, contributes to fructose–asparagine but not asparagine utilization, J. Bacteriol. 199 (2017) e00330-17.
[15] G.R. Richards, M.V. Patel, C.R. Lloyd, C.K. Vanderpool, Depletion of glycolytic intermediates plays a key role in glucose-phosphate stress in Escherichia coli, J. Bacteriol. 195 (2013) 4816–4825.
[16] A. Sabag-Daigle, J.K. Wu, M.A. Borton, A. Sengupta, V. Gopalan, K.C. Wrighton, et al., Identification of bacterial species that can utilize fructose–asparagine, Appl Environ Microb. 84 (2018) e01957-17.
[17] C.H. Baek, S.K. Farrand, K.E. Lee, D.K. Park, J.K. Lee, K.S. Kim, Convergent evolution of Amadori opine catabolic systems in plasmids of Agrobacterium tumefaciens, J. Bacteriol. 185 (2003) 513–524.
[18] V.M. Deppe, S. Klatte, J. Bongaerts, K.H. Maurer, T. O'Connell, F. Meinhardt, Genetic control of Amadori product degradation in Bacillus subtilis via regulation of frlBONMD expression by FrlR, Appl Environ Microb. 77 (2011) 2839–2846.
[19] K.S. Kim, S.K. Farrand, Ti plasmid-encoded genes responsible for catabolism of the crown gall opine mannopine by Agrobacterium tumefaciens are homologs of the T-region genes responsible for synthesis of this opine by the plant tumor, J. Bacteriol. 178 (1996) 3275–3284.
[20] E. Wiame, G. Delpierre, F. Collard, E. Van Schaftingen, Identification of a pathway for the utilization of the Amadori product fructoselysine in Escherichia coli, J. Biol. Chem. 277 (2002) 42523–42529.
[21] E. Wiame, A. Duquenne, G. Delpierre, E. Van Schaftingen, Identification of enzymes acting on alpha-glycated amino acids in Bacillus subtilis, FEBS Lett. 577 (2004) 469–472.
[22] E. Wiame, P. Lamosa, H. Santos, E. Van Schaftingen, Identification of glucoselysine-6-phosphate deglycase, an enzyme involved in the metabolism of the fructation product glucoselysine, Biochem. J. 392 (2005) 263–269.
[23] D. Joseph-McCarthy, L.E. Rost, E.A. Komives, G.A. Petsko, Crystal structure of the mutant yeast triosephosphate isomerase in which the catalytic base glutamic acid 165 is changed to aspartic acid, Biochemistry. 33 (1994) 2824–2829.
[24] J.R. Knowles, W.J. Albery, Perfection in enzyme catalysis: energetics of triosephosphate isomerase, Accounts Chem Res. 10 (1977) 105–111.
[25] R.T. Raines, E.L. Sutton, D.R. Straus, W. Gilbert, J.R. Knowles, Reaction energetics of a mutant triosephosphate isomerase in which the active-site glutamate has been changed to aspartate, Biochemistry. 25 (1986) 7142–7154.
[26] J.P. Richard, Acid–base catalysis of the elimination and isomerization-reactions of triose phosphates, J. Am. Chem. Soc. 106 (1984) 4926–4936.
[27] H. Roper, S. Roper, K. Heyns, B. Meyer, NMR-spectroscopy of N-(1-deoxy-D-fructos-1-Yl)-L-amino acids (fructose amino-acids), Carbohydr. Res. 116 (1983) 183–195.
[28] Y.F. Song, F. DiMaio, R.Y.R. Wang, D. Kim, C. Miles, T.J. Brunette, et al., High-resolution comparative modeling with RosettaCM, Structure. 21 (2013) 1735–1742.
[29] G. Ben-Nissan, M. Sharon, The application of ion-mobility mass spectrometry for structure/function investigation of protein complexes, Curr. Opin. Chem. Biol. 42 (2018) 25–33.
[30] F. Lermyte, E.M. Martin, A. Konijnenberg, F. Lemiere, F. Sobott, Native mass spectrometry approaches using ion mobility–mass spectrometry, in: J. Kool, W.M.A. Niessen (Eds.), Analyzing Biomolecular Interactions by Mass Spectrometry, Wiley-VCH, Weinheim, Germany, 2015, pp. 81–108.
[31] C. Bleiholder, T. Wyttenbach, M.T. Bowers, A novel projection approximation algorithm for the fast and accurate computation of molecular collision cross sections, Int. J. Mass Spectrom. 308 (2011) 1–10.
[32] E. Mack, Average cross-sectional areas of molecules by gaseous diffusion methods, J. Am. Chem. Soc. 47 (1925) 2468–2482.
[33] S. Harvey, Relative interfacial cleavage energetics of protein complexes revealed by surface collisions, Proc. Natl. Acad. Sci. (USA) 116 (2019) 8143–8148.
[34] Glide. 5.5 ed. New York: Schrodinger; 2009.
[35] M. Hernandez, D. Ghersi, R. Sanchez, SITEHOUND-web: a server for ligand binding site identification in protein structures, Nucleic Acids Res. 37 (2009) W413–W416.
[36] C.H. Ngan, T. Bohnuud, S.E. Mottarella, D. Beglov, E.A. Villar, D.R. Hall, et al., FTMAP: extended protein mapping with user-selected probe molecules, Nucleic Acids Res. 40 (2012) W271–W275.
[37] N.A. Yewdall, T.M. Allison, F.G. Pearce, C.V. Robinson, J.A. Gerrard, Self-assembly of toroidal proteins explored using native mass spectrometry, Chem. Sci. 9 (2018) 6099–6106.
[38] M. Peschke, U.H. Verkerk, P. Kebarle, Features of the ESI mechanism that affect the observation of multiply charged noncovalent protein complexes and the determination of the association constant by the titration method, J. Am. Soc. Mass Spectr. 15 (2004) 1424–1434.
[39] J.A. Silveira, K.L. Fort, D. Kim, K.A. Servage, N.A. Pierson, D.E. Clemmer, et al., From solution to the gas phase: stepwise dehydration and kinetic trapping of substance P reveals the origin of peptide conformations, J. Am. Chem. Soc. 135 (2013) 19147–19153.
[40] V.M. Monnier, X. Wu, Enzymatic deglycation with amadoriase enzymes from Aspergillus sp. as a potential strategy against the complications of diabetes and aging, Biochem. Soc. Trans. 31 (2003) 1349–1353.
[41] X. Wu, V.M. Monnier, Enzymatic deglycation of proteins, Arch. Biochem. Biophys. 419 (2003) 16–24.
[42] A. Teplyakov, G. Obmolova, M.A. Badet-Denisot, B. Badet, The mechanism of sugar phosphate isomerization by glucosamine 6-phosphate synthase, Protein Sci. 8 (1999) 596–602.
[43] J. Pierce, A.S. Serianni, R. Barker, Anomerization of furanose sugars and sugar phosphates, J. Am. Chem. Soc. 107 (1985) 2448–2456.
[44] J.K. Wu, A. Sabag-Daigle, M.A. Borton, L.F.M. Kop, B.E. Szkoda, B.L.D. Kaiser, et al., Salmonella-mediated inflammation eliminates competitors for fructose-asparagine in the gut, Infect. Immun. 86 (2018) e00945-17.
[45] T.A. Baillie, Targeted covalent inhibitors for drug design, Angew Chem Int Ed Engl. 55 (2016) 13408–13421.
[46] P. Conway, M.D. Tyka, F. DiMaio, D.E. Konerding, D. Baker, Relaxation of backbone bond geometry improves protein energy landscape modeling, Protein Sci. 23 (2014) 47–55.
[47] Schrodinger. 2.3 ed. New york: Ligprep; 2009.
[48] W. Humphrey, A. Dalke, K. Schulten, VMD: visual molecular dynamics, J. Mol. Graph Model. 14 (1996) 33–38.
[49] J.C. Phillips, R. Braun, W. Wang, J. Gumbart, E. Tajkhorshid, E. Villa, et al., Scalable molecular dynamics with NAMD, J. Comput. Chem. 26 (2005) 1781–1802.
[50] A.D. MacKerell, N. Banavali, N. Foloppe, Development and current status of the CHARMM force field for nucleic acids, Biopolymers. 56 (2001) 257–265.

[51] A.L. Hansen, E.J. Behrman, Synthesis of 6-phosphofructose aspartic acid and some related Amadori compounds, Carbohydr. Res. 431 (2016) 1–5.
[52] Z.L. VanAernum, J.D. Gilbert, M.E. Belov, A.A. Makarov, S.R. Horning, V.H. Wysocki, Surface-induced dissociation of noncovalent protein complexes in an extended mass range orbitrap mass spectrometer, Anal. Chem. 91 (2019) 3611–3618.
[53] M.T. Marty, A.J. Baldwin, E.G. Marklund, G.K. Hochberg, J.L. Benesch, C.V. Robinson, Bayesian deconvolution of mass and ion mobility spectra: from binary interactions to polydisperse ensembles, Anal. Chem. 87 (2015) 4370–4376.
[54] M.W. Zhou, S. Dagan, V.H. Wysocki, Protein subunits released by surface collisions of noncovalent complexes: nativelike compact structures revealed by ion mobility mass spectrometry, Angew. Chem. Int. Ed. 51 (2012) 4336–4339.
[55] S.J. Allen, K. Giles, T. Gilbert, M.F. Bush, Ion mobility mass spectrometry of peptide, protein, and protein complex ions using a radio-frequency confining drift cell, Analyst. 141 (2016) 884–891.
[56] M.F. Bush, Z. Hall, K. Giles, J. Hoyes, C.V. Robinson, B.T. Ruotolo, Collision cross sections of proteins and their complexes: a calibration framework and database for gas-phase structural biology, Anal. Chem. 82 (2010) 9557–9565.
[57] B.T. Ruotolo, J.L.P. Benesch, A.M. Sandercock, S.J. Hyung, C.V. Robinson, Ion mobility–mass spectrometry analysis of large protein complexes, Nat. Protoc. 3 (2008) 1139–1152.
[58] E.G. Marklund, M.T. Degiacomi, C.V. Robinson, A.J. Baldwin, J.L.P. Benesch, Collision cross sections for structural proteomics, Structure. 23 (2015) 791–799.
[59] J.L.P. Benesch, B.T. Ruotolo, Mass spectrometry: come of age for structural and dynamical biology, Curr. Opin. Struct. Biol. 21 (2011) 641–649.
[60] Z. Hall, A. Politis, M.F. Bush, L.J. Smith, C.V. Robinson, Charge-state dependent compaction and dissociation of protein complexes: insights from ion mobility and molecular dynamics, J. Am. Chem. Soc. 134 (2012) 3429–3438.
[61] C. Larriba-Andaluz, J. Fernandez-Garcia, M.A. Ewing, C.J. Hogan Jr., D.E. Clemmer, Gas molecule scattering and ion mobility measurements for organic macro-ions in He versus N2 environments, Phys. Chem. Chem. Phys. 17 (2015) 15019–15029.
[62] J.H. Miller, Experiments in Molecular Genetics, Cold Spring Harbor Laboratory, New York, 1972.
[63] M. Price-Carter, J. Tingey, T.A. Bobik, J.R. Roth, The alternative electron acceptor tetrathionate supports B-12-dependent anaerobic growth of Salmonella enterica serovar typhimurium on ethanolamine or 1,2-propanediol, J. Bacteriol. 183 (2001) 2463–2475.
[64] D.J. Warren, Preparation of highly efficient electrocompetent Escherichia coli using glycerol/mannitol density step centrifugation, Anal. Biochem. 413 (2011) 206–207.
[65] C.R. Reisch, K.L.J. Prather, The no-SCAR (Scarless Cas9 Assisted Recombineering) system for genome editing in Escherichia coli, Sci Rep-Uk. 5 (2015).
[66] R.N. Brown, J.A. Sanford, J.H. Park, B.L. Deatherage, B.L. Champion, R.D. Smith, et al., A comprehensive subcellular proteomic survey of Salmonella grown under phagosome-mimicking versus standard laboratory conditions, Int J Proteomics. 2012 (2012) 123076.